math xmlns="http://www.w3.org/1998/Math/MathML">mrow>mmultiscripts>mi mathvariant="normal">C/mi>mprescripts>/mprescripts>none>/none>mn>13/mn>/mmultiscripts>mo>(/mo>mi>n/mi>mo>,/mo>mn>2/mn>mi>n/mi>mi>γ/mi>mo>)/mo>mmultiscripts>mi mathvariant="normal">C/mi>mprescripts>/mprescripts>none>/none>mn>12/mn>/mmultiscripts>/mrow>/math> math xmlns="http://www.w3.org/1998/Math/MathML">mi>γ/mi>/math>-ray production in the 14–16 MeV incident neutron energy range

A. M. McEvoy, H. W. Herrmann, Y. Kim, T. S. Sedillo, H. Geppert-Kleinrath, C. R. Brune, T. N. Massey, A. V. Voinov, C. E. Parker, M. S. Rubery, and W. Stoeffl

Phys. Rev. C **103**, 064607 — Published 14 June 2021

DOI: 10.1103/PhysRevC.103.064607

^{13}C(n,2nγ)^{12}C Gamma Ray Production in the 14 - 16 MeV Incident Neutron Energy Range

A. M. McEvoy, H. W. Herrmann, Y. Kim, T. S. Sedillo, and H. Geppert-Kleinrath*
Los Alamos National Laboratory, Los Alamos, New Mexico 87545, USA

C. R. Brune, T. N. Massey, A. V. Voinov, and C. E. Parker†
Edwards Accelerator Laboratory, Ohio University, Athens, Ohio 45701, USA

M. S. Rubery and W. Stoeffl
Lawrence Livermore National Laboratory, Livermore, California 94550, USA
(Dated: April 28, 2021)

Gamma ray emission from ^{12}C and ^{13}C samples irradiated with deuterium-tritium fusion neutrons was experimentally measured at the Omega Laser Facility and at the Ohio University Edwards Accelerator Laboratory. The intent of these measurements was to determine the feasibility of using ^{13}C-based plastic ablators with embedded ^{12}C layers for dark mix diagnosis of inertial confinement fusion (ICF) implosions. Spectrally resolved measurements at Ohio University identified significant 4.44 MeV gamma ray emission from the ^{13}C(n,2nγ)^{12}C-L1 reaction channel. The recorded 4.44 MeV ^{13}C signal was compared against emission from an identically irradiated ^{12}C target with known ^{12}C(n,nγ)^{12}C-L1 cross section, which resulted in an average ^{13}C(n,2nγ)^{12}C-L1 cross section of 117 $\pm$ 17 mb over the incident neutron energy distribution range from 14.4 to 15.8 MeV. Integrated ^{13}C gamma ray signals above 2.9 MeV recorded with the Gas Cherenkov Detector (GCD-3) at Omega exceeded MCNP6.1 predictions by a factor of 3. The additional signal was attributed to 4.44 MeV gammas resulting in an inferred ^{13}C(n,2nγ)^{12}C-L1 cross section of 95 $\pm$ 11 mb at 14.1 MeV average incident neutron energy. As a result, the ^{13}Cbased dark mix diagnostic concept was deemed infeasible.

I. INTRODUCTION

Laser inertial confinement fusion (ICF) experiments at the National Ignition Facility (NIF) utilize indirect drive to implode spherical capsules filled with deuterium (D) and tritium (T) in an attempt to reach ignition. ICF implosions may be affected by a variety of phenomena that have deleterious effects on the compression and heating of the fuel, resulting in sub-optimal DT fusion yields. Instabilities are being continuously studied and efforts to diagnose and mitigate the resulting negative effects on target performance are an ongoing component of ICF fusion research.

One particularly detrimental phenomenon occurs when capsule ablator material is injected into the DT ice layer or central hot spot of the implosion, which rapidly cools the DT fuel and inhibits fusion burn. Existing diagnostics for this so called mix condition primarily rely on measurements of x-rays produced by heated ablator material and/or dopants that have been placed in the fuel or layered into the capsule prior to implosion [1–7]. Gamma rays from neutron interactions with ablator material may also be used to identify mix [8]. A condition known as dark mix may also occur, wherein a macroscopic quantity of ablator material mixes into the hot spot and degrades the implosion performance without reaching sufficient temperature to produce an x-ray signal indicative of mix. Consequently, additional diagnostic techniques must be developed in order to identify when dark mix has occurred.

One possible dark mix diagnostic technique involves utilizing a ^{13}C-based plastic capsule doped with a ^{12}C layer. If ablator material containing ^{12}C were mixed into the cryo-layered DT fuel or hotspot, the subsequent increase in the areal density (ρR) would lead to enhanced production of 4.44 MeV gamma rays from ^{12}C(n,nγ) inelastic scattering of 14.1 MeV DT neutrons, which could provide a positive indication of mix. In order for this concept to be feasible however, ^{13}C must not significantly emit gamma rays near or above 4.44 MeV when exposed to a similar mix environment as the doped ^{12}C.

MCNP6.1 (using the ENDF/B-VII data library) [9, 10] predicts ^{13}C gamma ray emission under ICF implosion conditions to be only from excitation of the first three excited states due to inelastic 14.1 MeV neutron scattering, with gamma ray energies of 3.09, 3.68, and 3.85 MeV. Spectral measurements of ^{13}C gamma ray production from 14.1 MeV neutron irradiation and the strength of other gamma emitting reaction channels, specifically ^{13}C(n,$\alpha\gamma$)^{10}Be and ^{13}C(n,2nγ)^{12}C, were not found during a literature search and appear not to have been experimentally determined. The first 5 excited states of ^{10}Be are above 3 MeV and below the neutron separation energy such that gamma ray emission from these states could pollute the mix signal. Similarly, if the ^{13}C(n,2nγ)^{12}C-L1 cross section is relatively large for producing ^{12}C in the first excited state, the subsequent emis-

* geppert@lanl.gov
† currently at: Cyclotron Institute, Texas A& M University, College Station, Texas 77843, USA.

sion of 4.44 MeV gammas would artificially increase the apparent ^{12}C mix signal and undermine the measurement.

This paper describes two experiments undertaken to identify gamma ray emission of ^{13}C under DT neutron irradiation, the resulting implications for using ^{12}C as a mix diagnostic and the inferred ^{13}C(n,2nγ)^{12}C-L1 cross section under two distinct measurements conditions.

II. SPECTRALLY INTEGRATED MEASUREMENTS WITH THE GAS CHERENKOV DETECTOR AT OMEGA

A. Experimental setup and data collection

Neutron induced gamma ray emission from ^{12}C and ^{13}C samples were measured using the newest iteration of the Gas Cherenkov Detector (GCD-3) [11, 12] at the Omega Laser Facility at the University of Rochester in Rochester, NY. Imploded targets consisted of 3.7 μm glass capsules with 10 atm equimolar DT fills producing an average DT neutron yield of 8.92×10^{13} over 6 shots, as measured with Cu-activation foils [13].

Two cylindrical (interior volume defined by 2.79 cm diameter, 0.914 cm depth) beryllium target holders, or pucks, were used to contain 99.9% isotopically enriched ^{12}C and ^{13}C powder samples, with a third empty puck used for determining the puck material contribution to the neutron induced gamma ray signal. Beryllium was chosen due to its low gamma ray production cross section in order to reduce the puck material gamma ray background. The pucks were mounted on thin aluminum stalks affixed to the front of the GCD-3, which placed the front face of the pucks approximately 6 cm from target chamber center (TCC). The time of flight for 14 MeV neutrons to reach the puck resulted in the neutron induced gamma ray signal peaking approximately 1.1 ns after the prompt gamma ray signal. The prompt gamma rays are primarily generated by DT fusion reactions as well as by neutron interactions with the SiO_2 ablator material.

The GCD-3 was pressurized with 400 psia CO_2, which yields a 2.9 MeV gamma ray energy threshold for producing observable Cherenkov photons in the detector. Gamma rays striking the front of the GCD-3 with energy above this threshold generate increasing quantities of Cherenkov photons with increasing gamma ray energy. The gamma ray response function for GCD-3 at 400 psia CO_2 is shown in Figure 1. This response function was generated utilizing a previously validated GEANT4 model [14] with the updated GCD-3 detector geometry and gas pressure. If only the first three excited states of ^{13}C are assumed to emit gamma rays under 14.1 MeV DT neutron irradiation and ^{12}C emits entirely from the first excited state at 4.44 MeV, then the predicted yield normalized ^{12}C/^{13}C GCD-3 signal ratio is 4.8.

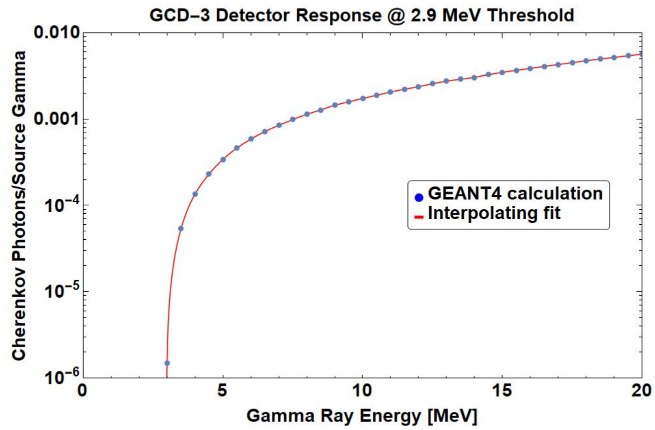

FIG. 1. GEANT4 simulation of GCD-3 (pressurized to 400 psia of CO_2) response function at various gamma ray energies (blue dots) with interpolating fit (red line).

B. Data analysis

Gamma ray signatures were recorded with 2 shots per puck for a total of 6 shots. The recorded GCD-3 signals were time aligned to the peak of the prompt gamma ray signal (scope bangtime), as shown in Figure 2. It can be seen that the puck signals are riding on top of a background signal that begins at ∼0.6 ns after bangtime, which is attributed to gamma rays from neutron interactions in the Neutron Wedge Range Filter (nWRF) diagnostic located 4 cm from TCC. An additional background signal is present that peaks around 1.7 ns that is attributed to neutron interactions in the Neutron Effects Diagnostic (NED) at 8.79 cm from TCC. All diagnostic locations were fixed across the 6 shots presented.

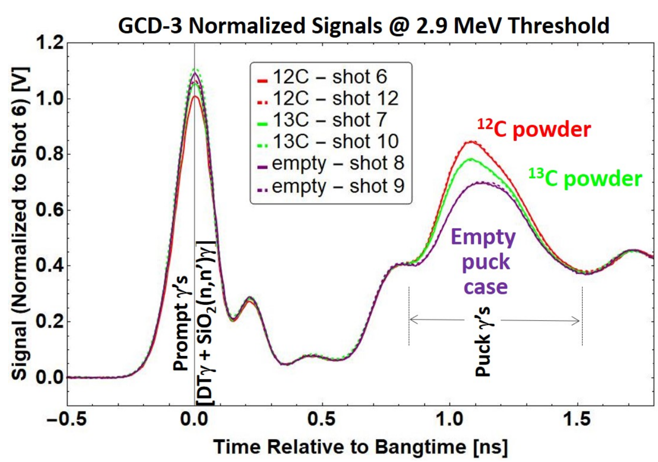

FIG. 2. Recorded GCD-3 gamma ray signals normalized using the neutron induced gamma ray signal feature located at ∼1.7 ns after bangtime.

Each shot was normalized to the amplitude of the NED background peak feature, which should be entirely yield dependent with minimal error because it is temporally separated from the puck signals and the NED was fixed across all 6 shots. This normalization procedure agreed with the Cu-activation yield measurements within a few percent on average, with the differences attributed to uncertainty in the Cu-activation measurement. Amplitude variations in the prompt gamma peak are due to shot-to-shot differences in compressed shell ρR during burn, which leads to varying quantities of prompt gamma ray production from neutron interactions with shell (SiO_2) material. All further discussion and results are based on these time aligned and normalized signals.

The pair of signals for each puck were averaged to obtain mean puck signal responses. The mean empty puck signal was subtracted from the mean ^{13}C and ^{12}C puck signals to remove the contribution from the beryllium cases and any additional background gamma ray signal. The ^{12}C signal was then scaled to account for the difference in target mass (5.93 g vs. 5.52 g of ^{13}C) and atomic mass (12 amu vs 13 amu for ^{13}C) in order to make an appropriate comparison. The resulting subtracted and corrected puck signals are overlaid in Figure 3.

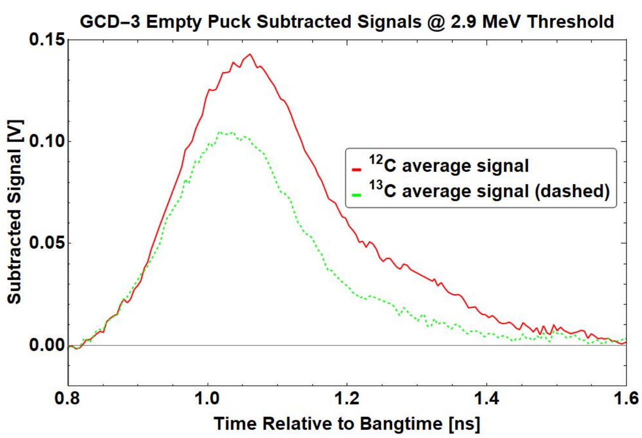

FIG. 3. Empty puck subtracted ^{12}C and ^{13}C puck gamma ray signals, each averaged over two feature-normalized GCD-3 recordings.

The background subtracted puck signals for each isotope were then integrated, representing the total gamma ray spectrum above 2.9 MeV. The ^{13}C sample produced $\sim$34% less integrated signal than the appropriately scaled ^{12}C sample resulting in a ^{12}C/^{13}C signal ratio of 1.51. This signal ratio corresponds to a ^{13}C signal a factor of $\sim$3$\times$ larger than predicted by MCNP6.1, which indicates that the first three ^{13}C excited states are not responsible for all of the observed signal. However, because the GCD-3 performs an energy-integrated measurement above the Cherenkov threshold a spectrally resolved gamma ray measurement was necessary to identify the specific reaction channel responsible for the additional gamma ray production.

III. GAMMA RAY SPECTRAL MEASUREMENTS AT OHIO UNIVERSITY

A. Experimental setup and data collection

Spectrally resolved gamma ray measurements of neutron irradiated ^{12}C (26.18 g) and ^{13}C (40.96 g) samples were performed at the Edwards Accelerator Laboratory at Ohio University in Athens, OH [15]. The facilitys 4.5 MeV tandem accelerator was used to direct a pulsed 500 keV deuteron beam onto a stopping tritiated titanium target to produce DT neutrons with a broad energy distribution with a forward-directed mean energy of 15.05 MeV (the simulated neutron energy spectrum is shown in Fig.8). The α particles from the DT reaction were monitored with a collimated Si detector located at 135° with respect to the incident deuteron beam. In this manner, the absolute DT neutron flux on the samples was determined within 3%. The pulses had a full-width at half maximum of 2.0 ns, with a 200 ns pulse period. Two small aluminum cans, filled with 99.95% isotopically enriched ^{12}C and 98% enriched ^{13}C powder [16] respectively, were placed $\sim$20 cm from the tritium target and irradiated with forward peaked neutrons.

A 10.16 cm diameter by 10.16 cm thick cylindrical Saint-Gobain BGO crystal mated to a PMT was placed at a distance of 4.46 m from the carbon targets with an angle of 90° between the axis of the deuteron beam and the axis of the BGO detector. The BGO detector viewed the targets through a 13 cm diameter aluminum collimator tube mounted within a 2 m thick shield wall constructed from layers of concrete, borated polyethylene and lead sheet. The detector was surrounded by multiple layers of lead bricks to minimize background gamma ray counts and a 2.5 cm thick borated polyethylene slab was placed directly in front of the BGO detector to minimize neutron interactions within the detector. Multiple layers of large paraffin blocks were stacked around the entrance of the collimator between the target and the shield wall in order to attenuate the neutron flux penetrating the wall. Tungsten blocks were also placed in the line of sight between the accelerator components surrounding the tritium target and the detector to minimize the amount of prompt neutron induced gamma rays impinging on the detector. GEANT4 simulations of the BGO detector give an efficiency of 2.52×10^{-5} with 10% uncertainty for a 3.0 MeV to 5.0 MeV gamma-ray point source at 4.46 m distance from the detector in air.

Data was collected by triggering the collection software on each pulse of deuterons striking the tritiated target in order to determine the time between a pulse and the recorded gamma rays. Prompt gamma rays produced in the target of interest arrived at the detector within a narrow time window such that counts at all other times were due to neutrons or time independent background (TIB) gamma rays from neutron interactions in non-target materials or from natural radioactive decay in the concrete time of flight (TOF) tunnel.

B. Data analysis

The energy axis for each data set was independently calibrated using the prominent background radiation lines at 1.46 MeV from natural ^{40}K decay and the 2.22 MeV line from hydrogen neutron capture in the paraffin and concrete shielding near the detector. The ^{12}C and ^{13}C data sets had prominent 4.44 MeV signals, which were also used for the energy axis calibration. A semi-log plot of the energy calibrated ^{12}C and ^{13}C spectra is shown in Figure 4.

A solid piece of aluminum of nearly the same dimension as the aluminum target cans was irradiated with neutrons and a gamma ray spectrum recorded. This aluminum spectrum was neutron rate normalized, scaled according to the mass of the cans and then subtracted from the neutron rate normalized ^{12}C and ^{13}C spectra.

The TIB gamma spectra for the ^{13}C and ^{12}C targets were sampled by selecting a set of counts with recorded TOF greater than the time window corresponding to gamma rays produced in the targets. The same number of time bins were chosen for the TIB spectra as were selected for the prompt gamma rays. The TIB spectra were then subtracted from the appropriate ^{12}C and ^{13}C data to generate the raw ^{12}C and ^{13}C spectra. The raw ^{12}C spectrum was then scaled to account for the difference in target mass (26.18 g vs 40.96 g) and atomic mass (12 amu vs 13 amu) between the ^{12}C and ^{13}C targets respectively.

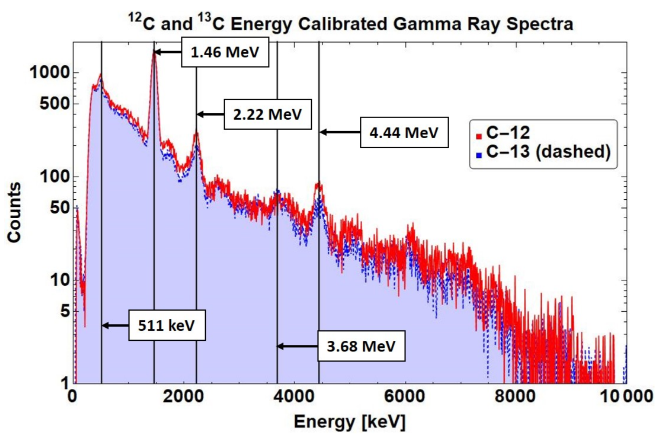

FIG. 4. Energy calibrated ^{12}C and ^{13}C spectra between 0 to 10 MeV. The 1.46 MeV ^{40}K decay line and the 2.22 MeV hydrogen neutron capture line are indicated, along with the observed 4.44 MeV gamma ray line from the ^{12}C and ^{13}C targets.

The relatively large 4.44 MeV gamma signal observed in the ^{13}C data set is of particular interest as it may explain the excess GCD-3 ^{13}C puck signal observed in the Omega data. The 4.44 MeV peaks in both the ^{12}C and ^{13}C data were isolated using a baseline correction to remove the Compton gamma ray continuum. The shape of the Compton continuum was determined using a piecewise linear fit to the baseline of the 4.44 MeV peak in a PuBe gamma ray spectrum (produced from ^{9}Be(α,nγ)^{12}C-L1 reactions) recorded using the same BGO detector as used for the ^{12}C and ^{13}C measurements. The Compton continuum baseline was matched to the baseline of the ^{12}C and ^{13}C spectra around the 4.44 MeV gamma ray peaks by scaling and vertically shifting the PuBe data by eye while keeping the areas under the peaks equal. This qualitative fitting approach introduces a conservatively estimated 10% uncertainty in the baseline subtracted peak counts used for ^{12}C/^{13}C signal comparison. The PuBe and ^{12}C gamma ray spectra with the matched Compton continuum baseline are shown in Figure 5 with the 4.44 MeV signal bracketed with vertical lines. The excess signal above background in the ^{12}C data between 3.0 - 3.8 MeV indicates the presence of additional unaccounted for gamma lines, however this signal does not affect the analysis of the 4.44 MeV peak. A similar plot of the ^{13}C gamma spectrum with PuBe data and matched baseline is shown in Figure 6.

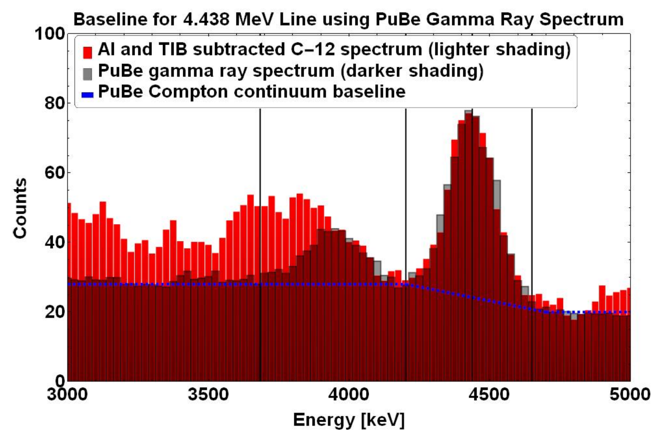

FIG. 5. Background subtracted ^{12}C spectrum between 3 to 5 MeV with overlaid PuBe 4.44 MeV peak, first escape peak and Compton continuum baseline.

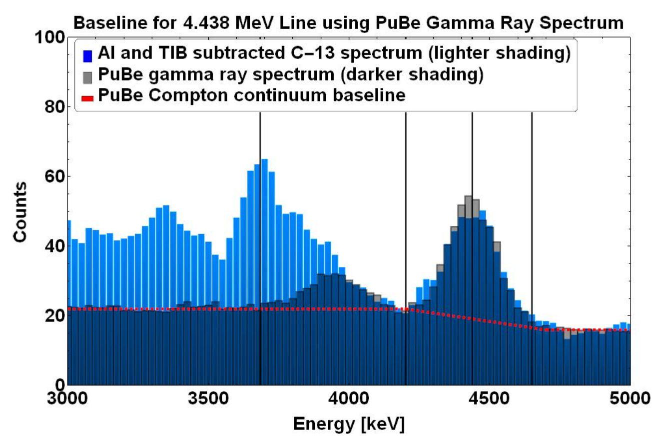

FIG. 6. Background subtracted ^{13}C spectrum between 3 to 5 MeV with overlaid PuBe 4.44 MeV peak, first escape peak and Compton continuum baseline.

The fully background corrected ^{12}C and ^{13}C spectra between 3 and 5 MeV are overlaid in Figure 7. The unique ^{13}C feature with peak between 3.6 and 3.7 MeV is primarily due to the 3.68 MeV gamma ray emitted by the 2^{nd} excited state of ^{13}C with additional contribution from the weaker 3^{rd} excited state at 3.85 MeV and from single-escape 4.44 MeV gammas at 3.93 MeV. The recorded ^{13}C counts in the energy range between 3.2 - 3.5 MeV may be evidence for 3.37 MeV gamma ray production from ^{13}C(n,$\alpha\gamma$)^{10}Be-L1 reactions, however it should be noted that the applied Compton baseline subtraction does not account for the effect of single-escape gammas from the 3.68 MeV and 3.85 MeV gammas that are present in this region.

Integrating the total signal in 4.44 MeV peaks results in a ^{13}C total gamma count ~32% lower than the corresponding ^{12}C gamma count yielding an observed ^{12}C/^{13}C signal ratio of 1.47 ± 0.19.

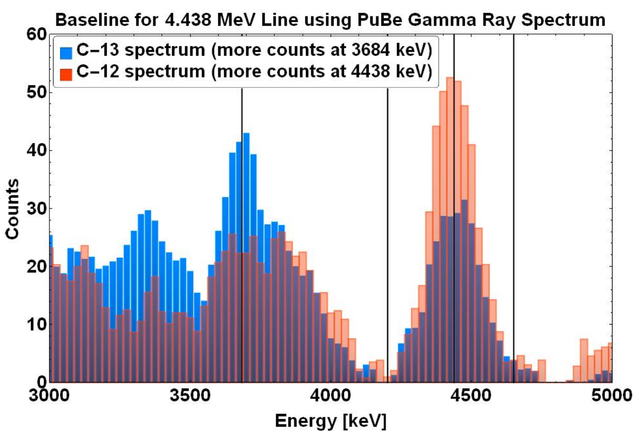

FIG. 7. Background and Compton baseline subtracted ^{12}C and ^{13}C gamma ray emission between 3 to 5 MeV.

IV. RESULTS

A. GCD-3 data at Omega

The JEFF3.3 listed 14.1 MeV neutron inelastic scattering cross sections for the first three excited states of ^{13}C [17] along with the corresponding gamma ray branching ratios [18] are tabulated in Table I. For a unit flux of 14.1 MeV neutrons on a ^{13}C target, the expected GCD-3 response to gamma rays emitted from the first three excited states is given by $R(^{13}C^{*})$ in Equation 1, where σ_{Li} is the cross section for populating the i^{th} excited state, BR_{Li-Lj} is the branching ratio for the gamma ray transition from the i^{th} to the j^{th} level and $R(\gamma)$ is the GCD-3 response to gamma rays from the indicated level transition. Equation 1 includes the expected signal contribution from all relevant gamma ray transitions but has been truncated here to show only the first four terms.

TABLE I. ^{13}C inelastic neutron scattering level population cross sections (σ) [17] and associated γ-ray production cross sections (σ_γ) [18].

σ (mb)	Initial Level	Final Level	γ-energy (MeV)	σ_γ (mb)
58	L3	L2	0.169	21.0
58	L3	L1	0.764	0.7
58	L3	L0	3.853	36.3
45	L2	L1	0.595	0.3
45	L2	L0	3.684	44.7
26	L1	L0	3.089	26.0

$$\begin{aligned}R(^{13}C^{*}) = &\sigma_{L1}BR_{L1-L0}R(\gamma_{L1-L0})+\\ &\sigma_{L2}BR_{L2-L1}R(\gamma_{L2-L1})+\\ &\sigma_{L2}BR_{L2-L1}BR_{L1-L0}R(\gamma_{L1-L0})+\\ &\sigma_{L2}BR_{L2-L0}R(\gamma_{L2-L0}) + ...\end{aligned} \tag{1}$$

Any additional GCD-3 signal from neutron reactions on ^{13}C can be represented by $R(^{13}C^{n,^*})$in Equation 2, where the neutron reaction cross section and branching ratio for the signal generating gamma ray have been grouped together as Φ_i for the i^{th} gamma ray.

$$R(^{13}C^{n,^*}) = \sum_i \Phi_i R(\gamma_i) \tag{2}$$

From the results of the Ohio University spectral measurement, the dominant contribution to the GCD-3 signal appears to be from 4.44 MeV gammas from the ^{13}C(n,2nγ)^{12}C-L1 reaction. The possible 3.37 MeV gamma contribution from ^{13}C(n,$\alpha\gamma$)^{10}Be-L1 reactions is assumed to be negligible due to the GCD-3 response at 4.44 MeV being ~9 times larger than at 3.37 MeV. Furthermore, all gamma rays with energies very near or below the 2.9 MeV threshold are assumed to produce negligible signal as the detector response at these energies is insignificant. Equation 2 then simplifies to Equation 3, assuming the additional GCD-3 signal is purely from 4.44 MeV gammas emitted from the ^{12}CL1 excited state with a branching ratio of 1.

$$R(^{13}C^{n,^*}) = \sigma_{^{13}C(n,2n\gamma)^{12}C-L1} R(4.44MeV) \tag{3}$$

The ^{12}C GCD-3 response, $R(^{12}C)$, to an equimolar ^{12}C target irradiated with unit 14.1 MeV neutron flux is given by Equation 4 using the total inelastic scatter cross section given by the ENDF/B-VII database value of 210 mb [18] and assuming that all gamma rays are emitted at 4.44 MeV with a branching ratio of 1.

$$R(^{12}C) = \sigma_{^{12}C(n,n'\gamma)^{12}C-L1} R(4.44MeV) \tag{4}$$

The observed GCD-3 ^{12}C/^{13}C signal ratio of 1.51 is then related to the ^{13}C(n,2nγ)^{12}CL1 cross section, $\sigma_{^{13}C(n,2n\gamma)^{12}C-L1}$, by Equation 5.

$$\frac{R(^{12}C)}{R(^{13}C^{*})+\sigma_{^{13}C(n,2n\gamma)^{12}C-L1}R(4.44MeV)}=1.51 \quad (5)$$

Rearranging terms and inserting known values into Equation 5 results in a measured cross section $\sigma_{^{13}C(n,2n\gamma)^{12}C-L1} = 95 \pm 11$ mb at 14.1 MeV average incident neutron energy.

The uncertainty in the $\sigma_{^{13}C(n,2n\gamma)^{12}C-L1}$ cross section is determined assuming a conservatively estimated 5% uncertainty in the GCD-3 average signal ratios, which includes both statistical and systematic uncertainties in the GCD-3 measurement. Uncertainty values for the JEFF3.3 listed ^{12}C and ^{12}C inelastic scatter cross sections are not tabulated and the gamma ray branching ratio uncertainties are 2% on average [18]. The uncertainty in the total gamma ray production cross sections from each ^{12}C and ^{13}C excited state are chosen to be 5% to account for measurement uncertainty in the JEFF3.3 data as well as the spread in neutron energies around 14.1 MeV due to Doppler broadening. A 10% uncertainty in the GEANT4 modeled GCD-3 response function is assumed for the full energy range of interest (2.9 - 5 MeV).

B. BGO data at Ohio University

The 90° differential cross section for ^{12}C(n,n'γ)^{12}C-L1 has been determined by taking into account the neutron energy distribution shown in Fig. 8 and the energy dependence of the of the ^{12}C(n,n'γ) cross section tabulated in ENDF/B-VII [18]. We find 13.8 ± 1.3 mb/sr at an average neutron energy of 15.05 MeV, where the uncertainty includes contributions from the neutron flux, BGO efficiency, neutron energy distribution, and the assumed energy dependence of the cross section. Anderson et al. [19] found the ratio of the 90° differential cross section to the average differential cross section to be 0.744. Using this factor, we determine the ^{12}C(n,n'γ)^{12}C-L1 cross section to be 233 ± 21 mb.

Using the measured ^{12}C/^{13}C 4.44-MeV gamma peak yield ratio of 1.47 ± 0.19 results in a ^{13}C(n,2nγ)^{12}C-L1 90° differential cross section of 9.39 ± 1.5 mb/sr. Assuming that the γ emission is isotropic results in $\sigma = 117 \pm 17$ mb.

C. Application to previously reported experiment

Hoffman [20] reported a gamma ray diagnostic technique for determining the ρR of the remaining ablator at bang-time for implosions utilizing CH-capsules with DT fuel fill. Data from two of the shots used in Hoffmans analysis were obtained from CH-capsule implosions

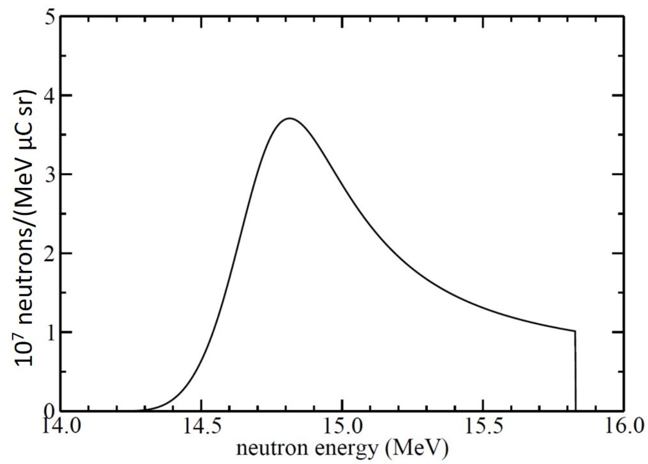

FIG. 8. Calculated forward directed neutron energy distribution incident upon the ^{12}C and ^{13}C targets.

where most of the carbon was enriched ^{13}C. The determined ρR value is linearly dependent on the strength of the 4.44 MeV gamma ray signal and ^{13}C was assumed to produce the same 4.44 MeV gamma ray signature as ^{12}C. The resulting observed ρR, as shown by the blue triangles in Figure 2 of [20], was about ∼40% lower on average than the calculated ρR values from 1D hydrodynamics simulations. Multiplying the measured ρR values for the two ^{13}C shots by the ^{12}C/^{13}C signal ratio of 1.51 described in Section II.B results in ρR values that are ∼12% lower on average than the calculated values, which is within the stated uncertainty ranges for both shots.

D. Cross section calculations

Cross sections of γ-transitions from n+^{13}C reactions at E_n=15.05 MeV have been calculated with the Empire nuclear reaction code [21] using the compound Hauser-Feshbach model [22]. We are aware that this model may not be wholly appropriate in this situation, due to the low level density in light nuclei. However, other options are lacking and this approach does incorporate many important physical considerations, including phase space and angular momentum and Coulomb barriers. Calculations show that dominant channels for this reaction are (n,n'), (n,2n), and (n,α) populating ^{13}C,^{12}C and ^{10}Be nuclei respectively. In its original form the Empire code is not able to calculate decay of particle-unstable dicrete levels and all discrete levels are assumed to decay by γ-radiation only. For ^{13}C, ^{12}C and ^{10}Be the discrete levels included only those below the particle separation thresholds of 4.9, 7.3, and 6.8 MeV respectively. Above the particle separation thresholds, the number of levels have been calculated with a level density approximation using the constant temperature model $\rho(E) = \frac{1}{T}e^{(E-E_0)/T}$. Parameters T and E_0 were adjusted in order to reproduce the number of experimentally identified discrete levels

TABLE II. Calculated γ-ray production cross sections (σ_γ) and their initial level population cross sections (σ) for ^{13}C inelastic neutron scattering.

σ (mb)	Initial Level	Final Level	γ-energy (MeV)	σ_γ (mb)
43.7	L3	L2	0.169	15.8
43.7	L3	L1	0.764	0.5
43.7	L3	L0	3.853	27.4
49.4	L2	L1	0.595	0.4
49.4	L2	L0	3.684	49.0
18.1	L1	L0	3.089	18.1

TABLE III. Calculated γ-ray production cross sections (σ_γ) and their initial level population cross sections (σ) for ^{13}C(n,α) channel populating ^{10}Be excited states.

σ (mb)	Initial Level	Final Level	γ-energy (MeV)	σ_γ (mb)
26.1	L5	L3	0.303	0.3
26.1	L5	L1	2.895	25.5
26.1	L5	L0	6.263	0.3
5.8	L4	L3	0.219	1.4
5.8	L4	L1	2.81	4.4
21.0	L3	L1	2.59	3.6
21.0	L3	L0	5.96	17.4
28.4	L2	L1	2.59	28.4
109.0	L1	L0	3.37	109.0

[23] up to 13.5, 18.4, and 13.8 MeV for ^{13}C,^{12}C, and ^{10}Be respectively. The resulting neutron absorption cross sections were calculated using the energy-independent spin cutoff parameters found from spin values of the known discrete levels and using the default optical model parameters of the Empire code.

For 15.05 MeV neutrons, the cross section of the ^{13}C(n,2nγ)^{12}C-L1$\rightarrow$L0 4.44 MeV γ-transition has been calculated to be 125 mb which is in good agreement with our experimental value of 117 $\pm$ 17 mb. Calculated cross section of other γ-transitions corresponding to inelastic (n,n') and (n,α) channels are presented in Tables II and III. The calculated cross sections in this work depend on various factors, in particular the choice of evaluated level populations from neutron inelastic scattering (e.g., JEFF3.3 vs ENDF/B-VIII). The ^{13}C(n,n'γ)-Lx cross sections were most similar between the Empire code calculations and the JEFF3.3 dataset while ENDF/B-VIII had significantly different values. As such the JEFF3.3 evaluated data was used for the calculations herein.

V. CONCLUSION

Gamma ray emission from DT neutron irradiated ^{12}C and ^{13}C samples was experimentally measured to determine the feasibility of using ^{13}C based CH ablators with embedded ^{12}C layers for dark mix diagnosis of ICF implosions. Spectrally integrated gamma ray measurements using the GCD-3 at Omega indicated that ^{13}C produced significantly more gamma rays above 2.9 MeV than was predicted by MCNP6.1 calculations. Spectrally resolved gamma ray measurements at Ohio University identified significant 4.44 MeV gamma ray production from the ^{13}C(n,2nγ)^{12}C-L1 reaction channel. The ratio of the recorded 4.44 MeV ^{12}C and ^{13}C signals combined with the known ^{12}C(n,nγ)^{12}C-L1 cross section over the incident neutron energy range resulted in a ^{13}C(n,2nγ)^{12}C-L1 cross section of 117 $\pm$ 17 mb. Attributing the additional gamma ray signal in the GCD-3 measurements to 4.44 MeV gammas resulted in a measured ^{13}C(n,2nγ)^{12}C-L1 cross section of 95 $\pm$ 11 mb at 14.1 MeV average incident neutron energy.

VI. ACKNOWLEDGEMENTS

The authors would like to acknowledge Alex Leatherland and Steve Gales from Atomic Weapons Establishment (AWE) for their assistance with experiments and data analysis. Special thanks to Reny Paguio from General Atomics for target assembly as well as Robert Haight from LANL for lending out the large ^{13}C sample. Finally, many thanks go to all of the staff and students at the Omega Laser Facility and at Ohio University for their support. This work was performed by the Los Alamos National Laboratory, operated by Triad National Security, LLC for the National Nuclear Security Administration (NNSA) of U.S. Department of Energy (DOE) under contract 89233218CNA000001.

[1] B. Hammel, S. Haan, D. Clark, M. Edwards, S. Langer, M. Marinak, M. Patel, J. Salmonson, and H. Scott, High-mode Rayleigh-Taylor growth in NIF ignition capsules, High Energy Density Phys. **6**, 171 (2010).

[2] S. P. Regan, R. Epstein, B. A. Hammel, L. J. Suter, H. A. Scott, M. A. Barrios, D. K. Bradley, D. A. Callahan, C. Cerjan, G. W. Collins, S. N. Dixit, T. Döppner, M. J. Edwards, D. R. Farley, K. B. Fournier, S. Glenn, S. H. Glenzer, I. E. Golovkin, S. W. Haan, A. Hamza, D. G. Hicks, N. Izumi, O. S. Jones, J. D. Kilkenny, J. L. Kline, G. A. Kyrala, O. L. Landen, T. Ma, J. J. MacFarlane, A. J. MacKinnon, R. C. Mancini, R. L. McCrory, N. B. Meezan, D. D. Meyerhofer, A. Nikroo, H.-S. Park, J. Ralph, B. A. Remington, T. C. Sangster, V. A. Smalyuk, P. T. Springer, and R. P. J. Town, Hot-spot mix in ignition-scale inertial confinement fusion targets, Phys. Rev. Lett. **111**, 045001 (2013).

[3] S. P. Regan, R. Epstein, B. A. Hammel, L. J. Suter, J. Ralph, H. Scott, M. A. Barrios, D. K. Bradley, D. A. Callahan, C. Cerjan, G. W. Collins, S. N. Dixit, T. Doeppner, M. J. Edwards, D. R. Farley, S. Glenn, S. H. Glenzer, I. E. Golovkin, S. W. Haan, A. Hamza, D. G. Hicks, N. Izumi, J. D. Kilkenny, J. L. Kline, G. A. Kyrala, O. L. Landen, T. Ma, J. J. MacFarlane, R. C. Mancini, R. L. McCrory, N. B. Meezan, D. D. Meyerhofer, A. Nikroo, K. J. Peterson, T. C. Sangster, P. Springer, and R. P. J. Town, Hot-spot mix in ignition-scale implosions on the NIF, Phys. Plasmas **19**, 056307 (2012), https://doi.org/10.1063/1.3694057.

[4] V. A. Smalyuk, M. Barrios, J. A. Caggiano, D. T. Casey, C. J. Cerjan, D. S. Clark, M. J. Edwards, J. A. Frenje, M. Gatu-Johnson, V. Y. Glebov, G. Grim, S. W. Haan, B. A. Hammel, A. Hamza, D. E. Hoover, W. W. Hsing, O. Hurricane, J. D. Kilkenny, J. L. Kline, J. P. Knauer, J. Kroll, O. L. Landen, J. D. Lindl, T. Ma, J. M. McNaney, M. Mintz, A. Moore, A. Nikroo, T. Parham, J. L. Peterson, R. Petrasso, L. Pickworth, J. E. Pino, K. Raman, S. P. Regan, B. A. Remington, H. F. Robey, D. P. Rowley, D. B. Sayre, R. E. Tipton, S. V. Weber, K. Widmann, D. C. Wilson, and C. B. Yeamans, Hydrodynamic instability growth and mix experiments at the National Ignition Facility, Phys. Plasmas **21**, 056301 (2014), https://doi.org/10.1063/1.4872026.

[5] V. A. Smalyuk, R. E. Tipton, J. E. Pino, D. T. Casey, G. P. Grim, B. A. Remington, D. P. Rowley, S. V. Weber, M. Barrios, L. R. Benedetti, D. L. Bleuel, D. K. Bradley, J. A. Caggiano, D. A. Callahan, C. J. Cerjan, D. S. Clark, D. H. Edgell, M. J. Edwards, J. A. Frenje, M. Gatu-Johnson, V. Y. Glebov, S. Glenn, S. W. Haan, A. Hamza, R. Hatarik, W. W. Hsing, N. Izumi, S. Khan, J. D. Kilkenny, J. Kline, J. Knauer, O. L. Landen, T. Ma, J. M. McNaney, M. Mintz, A. Moore, A. Nikroo, A. Pak, T. Parham, R. Petrasso, D. B. Sayre, M. B. Schneider, R. Tommasini, R. P. Town, K. Widmann, D. C. Wilson, and C. B. Yeamans, Measurements of an ablator-gas atomic mix in indirectly driven implosions at the National Ignition Facility, Phys. Rev. Lett. **112**, 025002 (2014).

[6] M. J. Edwards, P. K. Patel, J. D. Lindl, L. J. Atherton, S. H. Glenzer, S. W. Haan, J. D. Kilkenny, O. L. Landen, E. I. Moses, A. Nikroo, R. Petrasso, T. C. Sangster, P. T. Springer, S. Batha, R. Benedetti, L. Bernstein, R. Betti, D. L. Bleuel, T. R. Boehly, D. K. Bradley, J. A. Caggiano, D. A. Callahan, P. M. Celliers, C. J. Cerjan, K. C. Chen, D. S. Clark, G. W. Collins, E. L. Dewald, L. Divol, S. Dixit, T. Doeppner, D. H. Edgell, J. E. Fair, M. Farrell, R. J. Fortner, J. Frenje, M. G. Gatu Johnson, E. Giraldez, V. Y. Glebov, G. Grim, B. A. Hammel, A. V. Hamza, D. R. Harding, S. P. Hatchett, N. Hein, H. W. Herrmann, D. Hicks, D. E. Hinkel, M. Hoppe, W. W. Hsing, N. Izumi, B. Jacoby, O. S. Jones, D. Kalantar, R. Kauffman, J. L. Kline, J. P. Knauer, J. A. Koch, B. J. Koziozicmski, G. Kyrala, K. N. LaFortune, S. L. Pape, R. J. Leeper, R. Lerche, T. Ma, B. J. MacGowan, A. J. MacKinnon, A. Macphee, E. R. Mapoles, M. M. Marinak, M. Mauldin, P. W. McKenty, M. Meezan, P. A. Michel, J. Milovich, J. D. Moody, M. Moran, D. H. Munro, C. L. Olson, K. Opachich, A. E. Pak, T. Parham, H.-S. Park, J. E. Ralph, S. P. Regan, B. Remington, H. Rinderknecht, H. F. Robey, M. Rosen, S. Ross, J. D. Salmonson, J. Sater, D. H. Schneider, F. H. Sguin, S. M. Sepke, D. A. Shaughnessy, V. A. Smalyuk, B. K. Spears, C. Stoeckl, W. Stoeffl, L. Suter, C. A. Thomas, R. Tommasini, R. P. Town, S. V. Weber, P. J. Wegner, K. Widman, M. Wilke, D. C. Wilson, C. B. Yeamans, and A. Zylstra, Progress towards ignition on the National Ignition Facility, Phys. Plasmas **20**, 070501 (2013), https://doi.org/10.1063/1.4816115.

[7] O. A. Hurricane, D. A. Callahan, D. T. Casey, P. M. Celliers, C. Cerjan, E. L. Dewald, T. R. Dittrich, T. Dppner, D. E. Hinkel, L. F. B. Hopkins, J. L. Kline, S. L. Pape, T. Ma, A. G. MacPhee, J. L. Milovich, A. Pak, H.-S. Park, P. K. Patel, B. A. Remington, J. D. Salmonson, P. T. Springer, and R. Tommasini, Fuel gain exceeding unity in an inertially confined fusion implosion, Nature **506**, 343 (2014).

[8] C. Cerjan, D. B. Sayre, O. L. Landen, J. A. Church, W. Stoeffl, E. M. Grafil, H. W. Herrmann, N. M. Hoffman, and Y. Kim, Gamma Reaction History ablator areal density constraints upon correlated diagnostic modeling of National Ignition Facility implosion experiments, Phys. Plasmas **22**, 032710 (2015), https://doi.org/10.1063/1.4916124.

[9] J. Goorley, M. R. James, T. E. Booth, F. B. Brown, J. S. Bull, L. J. Cox, J. W. Durkee, J. S. Elson, M. L. Fensin, R. A. Forster, J. S. Hendricks, H. G. Hughes, R. C. Johns, B. C. Kiedrowski, R. L. Martz, S. G. Mashnik, G. W. McKinney, D. B. Pelowitz, R. E. Prael, J. Sweezy, L. S. Waters, T. Wilcox, and A. J. Zukaitis, *Initial MCNP6 Release Overview - MCNP6 version 1.0*, Tech. Rep. LA-UR-13-22934 (Los Alamos National Laboratory, 2013).

[10] M. Chadwick, P. Obloinsk, M. Herman, N. Greene, R. McKnight, D. Smith, P. Young, R. MacFarlane, G. Hale, S. Frankle, A. Kahler, T. Kawano, R. Little, D. Madland, P. Moller, R. Mosteller, P. Page, P. Talou, H. Trellue, M. White, W. Wilson, R. Arcilla, C. Dunford, S. Mughabghab, B. Pritychenko, D. Rochman, A. Sonzogni, C. Lubitz, T. Trumbull, J. Weinman, D. Brown, D. Cullen, D. Heinrichs, D. McNabb, H. Derrien, M. Dunn, N. Larson, L. Leal, A. Carlson, R. Block, J. Briggs, E. Cheng, H. Huria, M. Zerkle, K. Kozier, A. Courcelle, V. Pronyaev, and S. van der Marck, ENDF/B-VII.0: Next generation evaluated nuclear data library for nuclear science and technology, Nucl. Data Sheets **107**, 2931 (2006).

[11] H. W. Herrmann, Y. H. Kim, C. S. Young, V. E. Fatherley, F. E. Lopez, J. A. Oertel, R. M. Malone, M. S. Rubery, C. J. Horsfield, W. Stoeffl, A. B. Zylstra, W. T. Shmayda, and S. H. Batha, Extended performance gas Cherenkov detector for gamma-ray detection in high-energy density experiments, Rev. Sci. Instrum. **85**, 11E124 (2014), https://doi.org/10.1063/1.4892553.

[12] A. M. McEvoy, H. W. Herrmann, Y. Kim, A. B. Zylstra, C. S. Young, V. E. Fatherley, F. E. Lopez, J. A. Oertel, T. J. Sedillo, T. N. Archuleta, R. J. Aragonez, R. M. Malone, C. J. Horsfield, M. Rubery, S. Gales, A. Leatherland, W. Stoeffl, M. G. Johnson, W. T. Shmayda, and S. H. Batha, Gamma ray measurements at OMEGA with the newest gas Cherenkov detector "GCD-3", J. Phys. Conf. Ser. **717**, 012109 (2016).

[13] G. W. Cooper, C. L. Ruiz, R. J. Leeper, G. A. Chandler, K. D. Hahn, A. J. Nelson, J. A. Torres, R. M. Smelser, B. R. McWatters, D. L. Bleuel, C. B. Yeamans, K. M. Knittel, D. T. Casey, J. A. Frenje, M. Gatu Johnson, R. D. Petrasso, and J. D. Styron, Copper activation

deuterium-tritium neutron yield measurements at the National Ignition Facility, Rev. Sci. Instrum. **83**, 10D918 (2012), https://doi.org/10.1063/1.4746999.

[14] M. S. Rubery, C. J. Horsfield, H. Herrmann, Y. Kim, J. M. Mack, C. Young, S. Evans, T. Sedillo, A. McEvoy, S. E. Caldwell, E. Grafil, W. Stoeffl, and J. S. Milnes, Monte Carlo validation experiments for the gas Cherenkov detectors at the National Ignition Facility and Omega, Rev. Sci. Instrum. **84**, 073504 (2013).

[15] R. Finlay, C. Brient, D. Carter, A. Marcinkowski, S. Mellema, G. Randers-Pehrson, and J. Rapaport, The Ohio University beam swinger facility, Nucl. Instrum. Methods Phys. Res. **198**, 197 (1982).

[16] W. P. Abfalterer, F. B. Bateman, F. S. Dietrich, R. W. Finlay, R. C. Haight, and G. L. Morgan, Measurement of neutron total cross sections up to 560 MeV, Phys. Rev. C **63**, 044608 (2001).

[17] The Joint Evaluated Fission and Fusion File (JEFF-3.3), https://www.oecd-nea.org/dbdata/jeff/jeff33/index.html.

[18] F. Ajzenberg-Selove, Energy levels of light nuclei A = 1315, Nucl. Phys. A **523**, 1 (1991).

[19] J. D. Anderson, C. C. Gardner, J. W. McClure, M. P. Nakada, and C. Wong, Inelastic scattering of 14-MeV neutrons from carbon and beryllium, Phys. Rev. **111**, 572 (1958).

[20] N. M. Hoffman, H. W. Herrmann, Y. H. Kim, H. H. Hsu, C. J. Horsfield, M. S. Rubery, E. K. Miller, E. Grafil, W. Stoeffl, J. A. Church, C. S. Young, J. M. Mack, D. C. Wilson, J. R. Langenbrunner, S. C. Evans, T. J. Sedillo, V. Y. Glebov, and T. Duffy, Measurement of areal density in the ablators of inertial-confinement-fusion capsules via detection of ablator (n,n'γ) gamma-ray emission, Phys. Plasmas **20**, 042705 (2013), https://doi.org/10.1063/1.4799799.

[21] M. Herman, R. Capote, B. Carlson, P. Obloinsk, M. Sin, A. Trkov, H. Wienke, and V. Zerkin, EMPIRE: Nuclear reaction model code system for data evaluation, Nuclear Data Sheets **108**, 2655 (2007), Special Issue on Evaluations of Neutron Cross Sections.

[22] W. Hauser and H. Feshbach, The inelastic scattering of neutrons, Phys. Rev. **87**, 366 (1952).

[23] R. Capote, M. Herman, P. Obloinsk, P. Young, S. Goriely, T. Belgya, A. Ignatyuk, A. Koning, S. Hilaire, V. Plujko, M. Avrigeanu, O. Bersillon, M. Chadwick, T. Fukahori, Z. Ge, Y. Han, S. Kailas, J. Kopecky, V. Maslov, G. Reffo, M. Sin, E. Soukhovitskii, and P. Talou, RIPL reference input parameter library for calculation of nuclear reactions and nuclear data evaluations, Nuclear Data Sheets **110**, 3107 (2009), Special Issue on Nuclear Reaction Data.